Materials Advances

ROYAL SOCIETY OF CHEMISTRY

PAPER

View Article Online
View Journal | View Issue

Cite this: *Mater. Adv.*, 2025, 6, 3338

Strategies for balancing safety in oxadiazole tetrazole derivatives: the role of the oxime group†

Parul Saini,‡[a] Jatinder Singh,‡[a] Vikranth Thaltiri,[a] Richard J. Staples[b] and Jeanne M. Shreeve*[a]

Received 18th February 2025,
Accepted 15th April 2025

DOI: 10.1039/d5ma00150a

rsc.li/materials-advances

The development of modern thermostable and insensitive energetic materials is crucial. In this study, straightforward syntheses of thermostable and insensitive 4-amino-1,2,5-oxadiazol-3-yl(1*H*-tetrazol-5-yl)methanone oxime (**4**) and its energetic salts (**5–7**) are given. These oxime-bridged oxadiazole-tetrazole derivatives exhibit significant thermal stability, with decomposition temperatures 204–275 °C, and demonstrate high insensitivity to impact (IS > 40 J) and friction (FS > 360 N). These significant energetic performance properties can be ascribed to the oxime group positioned between the oxadiazole and tetrazole rings, which promotes robust non-covalent interactions within the molecular geometry. Moreover, the compounds exhibit favorable densities and high heats of formation compared to TNT, RDX, TATB, and HNS.

Introduction

Obtaining high molecular stability is a significant challenge in developing and utilizing energetic materials. Energetic materials are inherently sensitive to fluctuations in temperature, often resulting in premature ignition, degradation, or catastrophic failure when subjected to extreme thermal conditions. The prevalent approach for designing high-energy density materials (HEDMs) generally involves incorporating energy-rich functional groups, such as nitro ($-NO_2$), nitrato ($-ONO_2$), and nitramine ($-NHNO_2$), into nitrogen-rich heterocyclic frameworks. As the number of these groups increases through C- and N-functionalization, there is a corresponding enhancement in the density and performance of the resulting molecules. However, this improvement often comes with the challenge of reduced stability, making the compounds more difficult to handle safely during industrial production and storage. Balancing high energy output with stability demands a deeper understanding of nitrogen-rich compounds, making this field of research particularly complex and demanding.[1–5]

In this context, oxime-based energetic compounds have emerged as promising candidates due to their advanced thermal resistance and reduced sensitivity to external stimuli.[6–8] Despite being relatively underexplored, these compounds have garnered attention in the search for innovative, energetic materials capable of performing reliably under adverse conditions. The dehydrative cyclization of 1,2-dioximes to furazans and the oxidative cyclization to furoxans are two important synthetic strategies in energetic materials.[6] Both pathways generate compounds with considerable energetic potential, emphasizing the value of oxime chemistry in this field. These oxime-based compounds offer the potential for high enthalpies of formation and favorable densities, which are the key factors in designing efficient, energetic materials.

Previously oxime-based energetic compounds (Fig. 1b) were developed by incorporating nitrogen-rich energetic tetrazoles which show excellent thermal stability with good detonation velocities (**A**).[6] When the oxygen content was increased, the sensitivity of the compound increased (**B**).[7] Recently, our research group reported two highly thermostable and insensitive high-energy compounds: 1,2-di(1*H*-tetrazol-5-yl)ethane-1,2-dione dioxime (**C**) and dihydroxylammonium 1,2-di(1*H*-tetrazol-5-yl)ethane-1,2-dione (**D**). The oxime group in compound **D** acts as a H-bond donor and acceptor, enhancing the overall stability of the compound. Additionally, we discovered that the salt formation reaction between the oxime group and hydroxylamine maximized hydrogen bonding interactions, significantly improving the thermal resistance of the resulting compounds.[8]

The development of energetic materials based on five-membered nitrogen-containing heterocycles has become a focal point for scientists due to their energetic potential and intrinsic structural stability.[9] Among these heterocycles, azoles, oxadiazole, triazole, and tetrazole rings have emerged as leading candidates due to their high positive heats of formation (HOF).[10–14] These compounds contain energetic N–N, O–N, and C–N bonds, contributing to their energetic nature and stability.[15] 1,2,3-Triazole[16–18]

[a] *Department of Chemistry, University of Idaho, Moscow, Idaho, 83844-2343, USA. E-mail: jshreeve@uidaho.edu*
[b] *Department of Chemistry, Michigan State University, East Lansing, Michigan 48824, USA*

† Electronic supplementary information (ESI) available: Synthesis of compounds **4–7** and **12**, X-ray data of **6**, and isodesmic reactions, characterization data. CCDC 2413385. For ESI and crystallographic data in CIF or other electronic format see DOI: https://doi.org/10.1039/d5ma00150a

‡ Authors contributed equally.

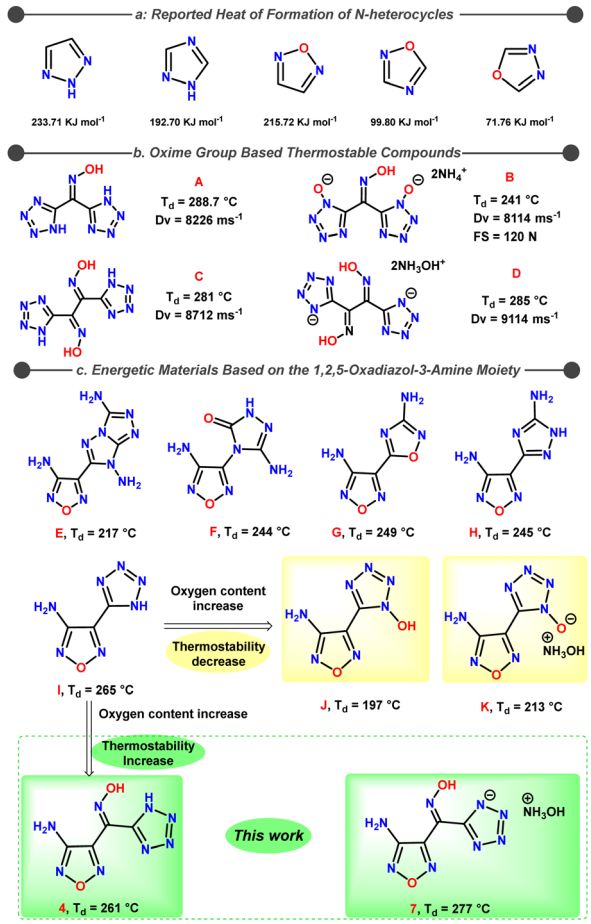

Fig. 1 (a) Reported heat of formation of N-heterocycles. (b) Oxime group based thermostable compounds. (c) Energetic materials based on the 1,2,5-oxadiazol-3-amine moiety and this work.

and 1,2,5-oxadiazole-based[19,20] compounds have shown more significant energetic promise due to their higher HOFs (Fig. 1a), making them ideal candidates for further development. In recent years, there have been numerous reports about the discovery of energetic compounds incorporating the 1,2,5-oxadiazol-3-amine moiety (Fig. 1c).[21–23] When the 1,2,5-oxadiazol-3-amine moiety is connected to a bicyclic fused ring (**E**), it exhibits a decomposition temperature of 217 °C.[21] However, when this moiety is linked to triazoles (**F**, **H**) and oxazoles (**G**), the decomposition temperature improves, ranging from 244 °C to 249 °C (Fig. 1c).[22,23] Incorporating the 1,2,5-oxadiazol-3-amine moiety into nitrogen-rich energetic tetrazoles (**I**) further enhances thermal stability, achieving an excellent decomposition temperature of 264 °C.[24] Conversely, increasing the oxygen content by connecting the 1,2,5-oxadiazol-3-amine moiety with tetrazol-1-ol (**J**) reduces thermal stability, resulting in a lower decomposition temperature of 197 °C.[25] This study addresses the challenge of reduced thermal stability associated with increased oxygen content in 1,2,5-oxadiazol-3-amine-tetrazole derivatives (**J**, **L**). When an oxime group is inserted between the tetrazole and oxadiazole rings (**4**, **7**), a balanced combination of enhanced thermal stability and improved safety in the energetic material compounds is achieved (Fig. 1c).

Building on these findings, we have also explored new compounds that combine oxime groups with tetrazole and 1,2,3-triazole rings. This work evaluates how these structural modifications influence the thermal stability, sensitivity, and energy output of these advanced materials.

Results and discussion

The synthetic route for 4-amino-1,2,5-oxadiazol-3-yl(1*H*-tetrazol-5-yl)methanone oxime (**4**) is outlined in Scheme 1. The process begins with the diazotization of 4-amino-*N*′-hydroxy-1,2,5-oxadiazole-3-carboximidamide (**1**) in aqueous hydrochloric acid with $NaNO_2$, yielding the intermediate chloroxime (**2**). A chloro–cyanide exchange of **2** with KCN produces **3**, which is further reacted with sodium azide in the presence of an aqueous solution to give **4**. The ammonium salt (**5**) is synthesized subsequently by treating **4** with aqueous ammonia. In addition, energetic salts **6**, and **7** were prepared by reacting compound **4** with hydrazine, and hydroxylamine (50% in water) in methanol respectively.[26]

The synthesis of compound **12**, which features an oxime group attached to tetrazole and 1,2,3-triazole rings, is shown in Scheme 2. The preparation of **10** followed a literature procedure.[27] Treatment of **10** with potassium cyanide (KCN) at room temperature facilitated the substitution of the chlorine atom with a cyanide group, resulting in 11 in good yield. Further reaction of **11** with sodium azide and zinc chloride in an aqueous solution led to the formation of **12**.

Crystallography

Despite our efforts, we were unable to obtain single crystals of compound **4** suitable for X-ray diffraction analysis. Therefore, direct experimental determination of the intermolecular interactions in the neutral compound is not possible at this time. While the crystal structure of **4** remains elusive, we reasoned that analyzing the crystal structure of its readily available hydrazinium salt, **6**, could still provide valuable, albeit indirect, insights. The core molecular framework of **4**, featuring the oxime group connecting the oxadiazole and tetrazole rings, is preserved in **6**. Although the protonation and the presence of

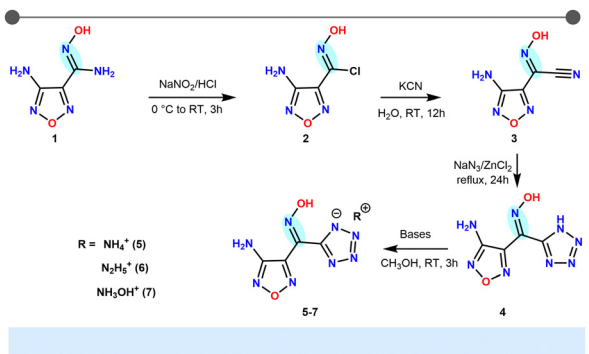

Scheme 1 Synthesis of compound 4-amino-1,2,5-oxadiazol-3-yl(1*H*-tetrazol-5-yl)methanone oxime (**4**) and its energetic salts (**5–7**).

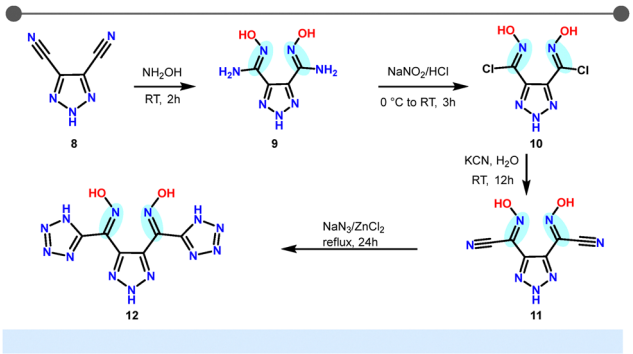

Scheme 2 Synthesis of energetic compound **12**.

the hydrazinium counterion introduce additional strong hydrogen bonds, the relative spatial arrangement of the oxime, oxadiazole, and tetrazole moieties is expected to be qualitatively similar in both compounds. This similarity allows us to use the analysis of **6** as a reasonable proxy for understanding the potential types of interactions that might be present in **4**, particularly those involving the oxime group.

Suitable crystals of compound **6** were obtained by the slow evaporation of water. The hydrazinium salt **6** crystallizes in the monoclinic $P2_1/n$ space group. In the crystal structure, the oxadiazole ring and oxime groups are found to be coplanar, while the tetrazole ring is in a different plane (Fig. 2A and B). The torsion angles are O2–N4–C3–C4 = −0.84(15) and O2–N4–C3–C2 = 179.99(9), respectively. At 100 K, the calculated density for compound **6** is 1.63 g cm^{-3}. The inter− and intramolecular hydrogen bonding between the hydrazinium cation with tetrazole rings and oxygen of oximes is shown in Fig. 2C. The oxime hydrogen shows the intermolecular hydrogen bonding with tetrazole ring with a distance of 1.84 Å which resembles the significant interaction of oxime group in the molecular system.

A detailed discussion of hydrogen bonding is given in Table S1.7 (ESI†). The hydrogen bonding interactions with a maximum D–D distance of 3.1 Å and a minimum angle of 110° are present in **6**. In the crystal packing structure, non-covalent interactions may include contributions from π-stacking. The crystal packing diagram shows layered packing with the intermolecular distance layers in the range of 3.147 Å (Fig. 2D).

To better understand the relationship between molecular structures and their physical characteristics, Hirshfeld surfaces and 2D fingerprints were examined. Fig. 3 presents the Hirshfeld surface and 2D fingerprint plot for compound **6** using the CrystalExplorer 21.5 software. The red sites are due to the intermolecular hydrogen bond interactions, and the blue spots for C···O, C···C, and C···N bond interactions explain possible π-stacking interactions (Fig. 3A). As expected for a hydrazinium salt, the analysis is dominated by features associated with strong hydrogen bonding. Fig. 3A clearly indicates the intermolecular hydrogen bonding with the tetrazole ring of another molecule. Due to the hydrogen bonding interaction, it forms sheet-like 3D framework. The prominent spikes in the fingerprint plot correspond to N–H···O and N–H···N contacts. The total H-bond interactions, O–H/N and N–H/N, is 66.4% (Fig. 3B and C). The larger value of these stabilizing interactions enhances molecular stability and insensitivity of 6. In the 2D fingerprint plot, the percentage of C–O, N–N, and N–C interaction (Fig. 3D–F) is 12.9%, indicating the potential π-stacking contributions between the molecules. Since π–π-stacking interactions play an important role in reducing the sensitivity towards friction, the occurrence of these interactions between the molecules was further visualized by drawing a NCIs (non-covalent interactions) plot (Fig. 3H). The green surface can be clearly seen from the figure and is due to the potential π-stacking contributions. These interactions give rise to good temperature resistance and insensitivity to external stimuli. By plotting the distribution of localized orbital locator-π (LOL-π) electrons, electron clouds are found in most of the atoms of compound **6** (Fig. S3B, ESI†).

This phenomenon helps to explain its low sensitivity. While this analysis is specific to the salt, it highlights the strong

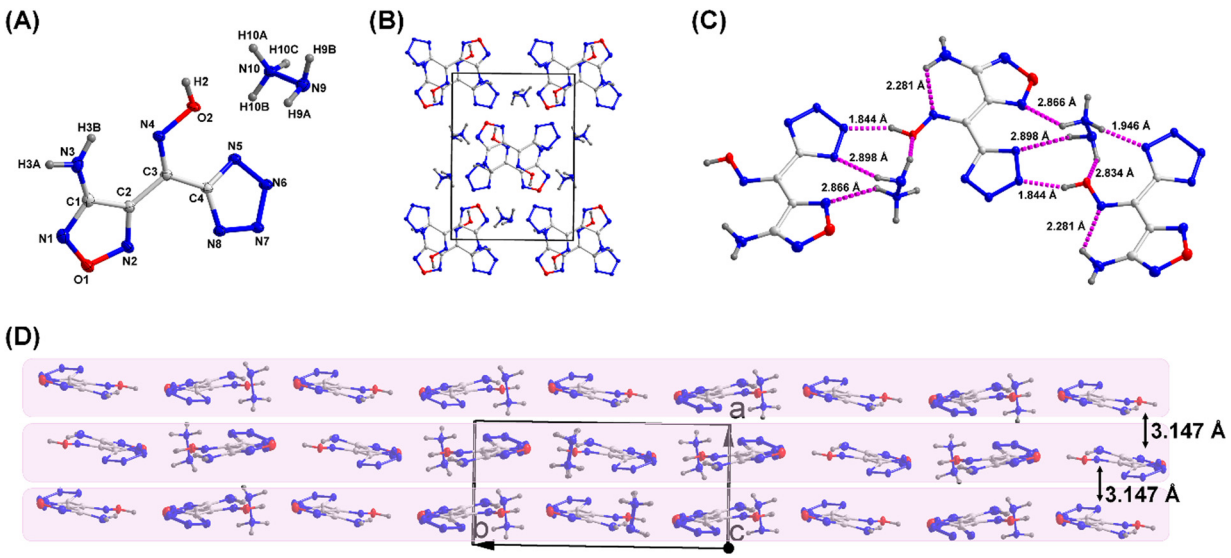

Fig. 2 (A) Tagging scheme of **6**. (B) Packing diagram of **6**. (C) Hydrogen bond networks in **6**. (D) Packing diagram of **6**.

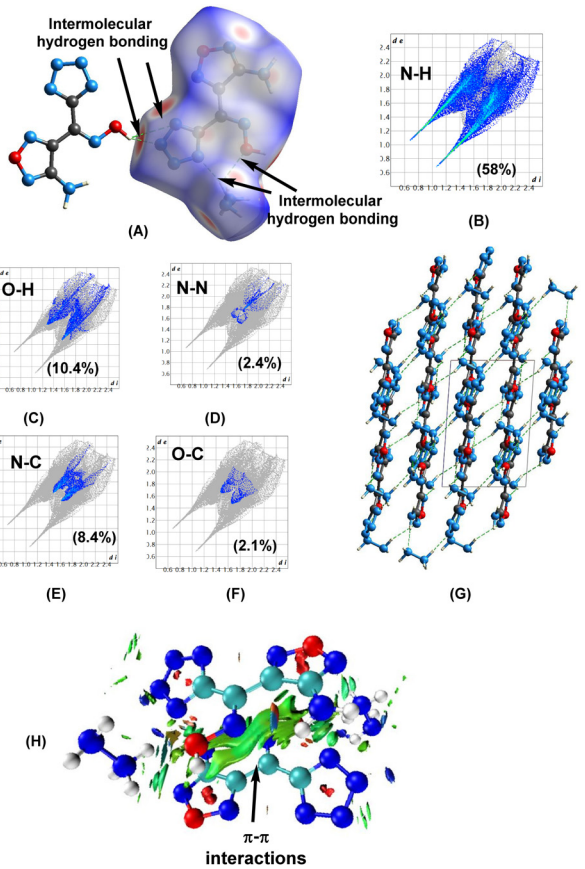

Fig. 3 (A)–(F) Hirshfeld surfaces and 2D fingerprint plots for 6, (G) hydrogen bonding enable 3D framework for **6**. (H) NCI plot for **6**.

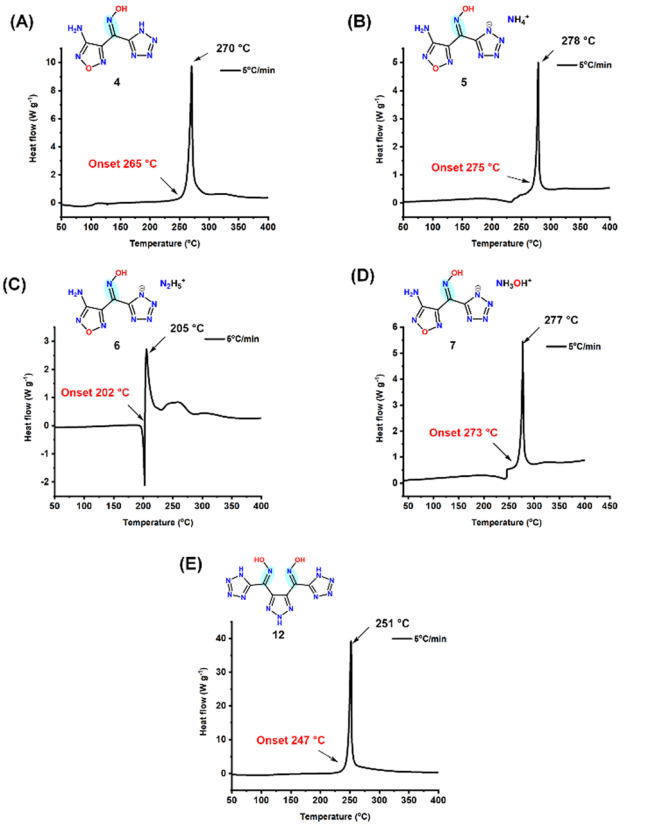

Fig. 4 DSC analysis at the heating rate of 5 °C min^{-1} (A) **4**. (B) **5**. (C) **6**. (D) **7**. (E) **12**.

propensity of this molecular system to engage in hydrogen bonding, a characteristic that is also likely to be important in the neutral compound, **4**, particularly involving the oxime group. For more clarity regarding interactions present in compound **4**, the NCl plot and LOL-π diagram are illustrated in Fig. S2 and S3A (ESI†). The NCl plots highlight the noncovalent interactions present in compound **4**, which may contribute to increased crystal density while reducing IS and FS. Additionally, the LOL-π diagrams reveal a widespread distribution of π-electrons throughout most of the structure. This conjugation enhances the molecular stability, leading to improved thermal stability and reduced sensitivity.

Physicochemical and detonation properties

The thermal behaviour of compounds **4**, **5**, **6**, **7**, and **12** was analyzed using DSC scans at a heating rate of 5 °C min^{-1} under an N_2 atmosphere (Fig. 4, Table 1). Among these, the ammonium salt (**5**) exhibited the highest decomposition temperature, recorded at 275 °C on the DSC. The decomposition temperatures of compounds **4**, **7**, and **12** are 265 °C, 273 °C, and 247 °C, respectively. Notably, compound **6** displayed an exothermic peak temperature (T_d) of 205 °C. The excellent thermal stability of these compounds can be attributed to strong hydrogen bonding interactions. The impact and friction sensitivities of compounds **4**–**7** and **12** were assessed using BAM standard methods, as summarized in Table 1. All these compounds demonstrated very low sensitivity to impact (>40 J) and friction (>360 J). The experimental densities of various compounds were determined using a gas pycnometer at a controlled temperature of 25 °C. Compounds **5** and **7** notably displayed similar calculated densities to trinitrotoluene (TNT), while compound **12** exhibited a density greater than both TNT and hexanitrostilbene (HNS). In conjunction with density measurements, enthalpies of formation (ΔH_f) were calculated and are given in Table 1. Compound **4** has an enthalpy of formation of 108.8 kJ mol^{-1}. In contrast, the energetic salts **5**, **6**, and **7** exhibited significantly higher positive enthalpies of formation at 470.0, 625.5, and 522.4 kJ mol^{-1}, respectively. These values exceed those of HNS, TNT, RDX, and triaminotrinitrobenzene (TATB), indicating a substantial potential for energetic performance due to their higher formed energy content. The experimental densities and calculated enthalpies of formation were utilized with EXPLO5 (v7.01.01) software to predict the detonation properties of these compounds. The results indicate that compound **6** has the highest calculated detonation velocity at 8071 m s^{-1}, positioning it as a formidable candidate, closely rivaling that of TATB. Furthermore, compounds **5**, **6**, and **7** exhibited detonation velocities that surpassed those of both TNT and HNS, which indicates their enhanced explosive characteristics (Table 1).

Conclusions

Thermostable and insensitive high-energy compound, 4-amino-1,2,5-oxadiazol-3-yl(1*H*-tetrazol-5-yl)methanone oxime (**4**) and

Table 1 Physicochemical properties of compounds **4–7**, **12**

Comp.	T_m[a] (°C)	T_d[b] (°C)	OB_{CO/CO_2} (%)	N [%]	ρ[c] (g cm^{-3})	ΔH_f[d] (kJ mol^{-1})	P[e] (GPa)	D_v[f] (ms^1)<	IS[g] (J)	FS[h] (N)
4	—	265	−10.7/−39.2	57	1.62	108.8	14.6	6561	>40	>360
5	206	275	−10.2/−36.5	59	1.65	470.0	23.0	7963	>40	>360
6	198	202	−10.2/−35.39	61	1.61	625.5	23.6	8071	>40	>360
7	218	273	−1.8/−25.7	55	1.65	522.4	23.6	8037	>40	>360
12	—	247	−17.61/−46.7	62	1.75	601.4	20.2	7479	>40	>360
J	—	189	—/−47.1	57	1.73	441.0	30.0	8601	37	>360
K	—	213	—/47.5	55	1.82	454.5	33.4	9100	>50	>360
TNT[i]	—	295	−24.6/−73.9	18	1.65	68.0	19.5	6881	15	353
HNS[j]	—	318	5.2/−37.9	18	1.75	78.0	24.3	7612	5	240
TATB[k]	—	350	10.5/−21.0	32	1.93	−139.7	30.5	8179	>40	360
RDX[l]	—	204	—/−21.6	37	1.80	92.6	34.9	8795	7.5	120

[a] Temperature melting. [b] Temperature (onset) of decomposition. [c] Density at 25 °C using gas pycnometer. [d] Molar enthalpy of formation, calculated using isodesmic reactions with the Gaussian 03 suite of programs (revision D.01). [e] Detonation pressure. [f] Detonation velocity (calculated using EXPLO5 version 7.01.01). [g] Sensitivity to impact (IS). [h] Sensitivity to friction (FS). All compounds were anhydrous powders for determination of properties in Table 1. [i] Ref. 28. [j] Ref. 29. [k] Ref. 30. [l] Ref. 31.

its energetic salts (**5–7**), were synthesized through straightforward steps starting from compound **1**. The molecular structure of compound **6** was confirmed by single-crystal X-ray crystallography. These compounds exhibit noteworthy thermal stability (decomposition temperatures >204 °C) and are highly insensitive to impact and friction (IS > 40 J, FS > 360 N), which can be attributed to robust inter- and intramolecular hydrogen bonding interactions. In addition to their excellent thermal and mechanical properties, these compounds possess good density and high heats of formation compared to TNT, RDX, TATB, and HNS. Furthermore, their compatibility with other energetic materials enhances their potential as promising candidates for new high-energy-density materials with practical applications.

Data availability

All data relevant to the work described here are available in the ESI,† or from the CCDC.†

Conflicts of interest

There are no conflicts to declare.

Acknowledgements

The diffractometer (Rigaku Synergy S) for SC-XRD was purchased with support from the National Science Foundation (MRI program) under grant no. 1919565. We are grateful to the Fluorine-19 fund for support. The authors thank Prof. Haixiang Gao, Department of Applied Chemistry, College of Science, China Agricultural University, Beijing, China for fruitful discussions.

References

1 C. Zhang, J. Huang and R. Bu, *Intrinsic structures and properties of energetic materials*, Springer Nature, 2012.
2 K. Zhong and C. Zhang, *Chem. Eng. J.*, 2024, **483**, 149202.
3 J. Zhang, Y. Feng, Y. Bo, R. J. Staples, J. Zhang and J. M. Shreeve, *J. Am. Chem. Soc.*, 2021, **143**, 12665–12674.
4 Y. H. Joo and J. M. Shreeve, *Org. Lett.*, 2008, **10**, 4665–4667.
5 M. A. Ilyushin, I. V. Tselinsky and I. V. Shugalei, *Cent. Eur. J. Energ. Mater.*, 2012, **9**, 293–328.
6 D. Chand, D. A. Parrish and J. M. Shreeve, *J. Mater. Chem. A*, 2013, **1**, 15383–15389.
7 G. Zhao, C. He, P. Yin, G. H. Imler, D. A. Parrish and J. M. Shreeve, *J. Am. Chem. Soc.*, 2018, **140**, 3560–3563.
8 J. Singh, R. J. Staples and J. M. Shreeve, *J. Mater. Chem. A*, 2023, **11**, 12896–12901.
9 A. A. Dippold, D. Izsak, T. M. Klapötke and C. Pfluger, *Chem. – Eur. J.*, 2016, **22**, 1768–1778.
10 J. Ma, A. K. Chinnam, G. Cheng, H. Yang, J. Zhang and J. M. Shreeve, *Angew. Chem., Int. Ed.*, 2021, **133**, 5557–5564.
11 J. Ma, Y. Tang, G. Cheng, G. H. Imler, D. A. Parrish and J. M. Shreeve, *Org. Lett.*, 2020, **22**, 1321–1325.
12 Q. Yu, P. Yin, J. Zhang, C. He, G. H. Imler, D. A. Parrish and J. M. Shreeve, *J. Am. Chem. Soc.*, 2017, **139**, 8816–8819.
13 Y. Tang, L. A. Mitchell, G. H. Imler, D. A. Parrish and J. M. Shreeve, *Angew. Chem., Int. Ed.*, 2017, **56**, 5894–5898.
14 Y. Zhou, H. Gao and J. M. Shreeve, *Energy Mater Front.*, 2020, **1**, 2–15.
15 Z. Dong and Z. Ye, *J. Mater. Chem. A*, 2020, **8**, 25035–25039.
16 C. He and J. M. Shreeve, *Angew. Chem., Int. Ed.*, 2015, **54**, 6260–6264.
17 Y. Cao, H. Huang, L. Wang, X. Lin and J. Yang, *J. Org. Chem.*, 2023, **88**, 4301–4308.
18 S. Feng, Y. Li, Q. Lai, J. Cai, Z. Wang, P. Yin, C. He and S. Pang, *Chem. Eng. J.*, 2022, **430**, 133181.
19 Y. Tang, J. Zhang, L. A. Mitchell, D. A. Parrish and J. M. Shreeve, *J. Am. Chem. Soc.*, 2015, **137**, 15984–15987.
20 C. Yan, K. Wang, T. Liu, H. Yang, G. Cheng and Q. Zhang, *Dalton Trans.*, 2017, **46**, 14210–14218.
21 C. Lei, H. Yang, Q. Zhang and G. Cheng, *Dalton Trans.*, 2021, **50**, 14462–14468.
22 Y. Liu, Z. Zeng, W. Huang, J. M. Shreeve and Y. Tang, *J. Org. Chem.*, 2022, **87**, 4226–4231.
23 Y. Tang, G. H. Imler, D. A. Parrish and J. M. Shreeve, *Org. Lett.*, 2018, **20**, 8039–8042.

24 B. Wang, G. Zhang, H. Huo, Y. Fan and X. Fan, *Chin. J. Chem.*, 2011, **29**, 919–924.
25 J. Zhang, L. A. Mitchell, D. A. Parrish and J. M. Shreeve, *J. Am. Chem. Soc.*, 2015, **137**, 10532–10535.
26 M. A. Epishina, A. S. Kulikov and N. N. Makhova, *Russ. Chem. Bull.*, 2008, **57**, 644–651.
27 Q. Zhang, C. He and S. Pang, *New J. Chem.*, 2022, **46**, 14324–14327.
28 X.-E. Jiang, B. Wu, B. Yang, Z.-C. Zhang, Y.-L. Yang, H.-Y. Du and C.-M. Ma, *Energy Mater. Front.*, 2023, **4**, 68–76.
29 X. Yu, J. Tang, C. Lei, H. Yang and G. Cheng, *Cryst. Growth Des.*, 2024, **24**, 455–460.
30 C. Zhang, H. Zhang, M. Xu, Z.-J. Lu, W.-S. Dong, T. Wang, X. Wu, Z. Li and J.-G. Zhang, *Cryst. Growth Des.*, 2024, **24**, 3160–3169.
31 Y. Tang, C. He, L. A. Mitchell, D. A. Parrish and J. M. Shreeve, *J. Mater. Chem. A*, 2016, **4**, 3879–3885.